Liquid crystal blazed grating beam deflector

Xu Wang[a], Daniel W. Wilson[b], Richard E. Muller[b], Paul D. Maker[b], Demetri Psaltis[a]

[a]MS 136-93, Department of Electrical Engineering
California Institute of Technology
Pasadena, CA 91125, USA

[b]Center for Space Microelectronics Technology
Jet Propulsion Laboratory
California Institute of Technology
Pasadena, CA 91109-8099, USA

ABSTRACT

A multiple-angle liquid crystal blazed grating beam deflector has been developed. It consists of a stack of liquid crystal blazed gratings where each layer can deflect incident light with very high efficiency into one of two different directions depending on the driving condition. Four steering angles (10.8°, 7.2°, 3.6°, 0°) with about 70% diffraction efficiency are demonstrated within 15V. The device's working principle, design considerations, fabrication process, and characterization results are described.

Keywords: beam steering, liquid crystal devices, diffractive optics

1. INTRODUCTION

A non-mechanical beam steering device is an important component in many applications, such as optical interconnects, optical communications, projection displays, and optical data storage. However, beam deflectors that are commercially available or are in development require either high operating voltage[1] or complicated fabrication technology.[2] The resulting devices are expensive, bulky, and exhibit high power consumption. In many applications, low cost and especially low power consumption are desired. One solution is to make a liquid crystal deflector since it can operate at low voltage and potentially can be low cost.

In this paper, a non-mechanical beam steering device using nematic liquid crystal (LC) is introduced. Although the target application is a holographic memory system, this device is also a good candidate for many other applications, such as fiber communications, micro-displays, and optical scanners. The paper is organized as follows. The operating principles and design considerations are described in Section 2; the fabrication process is described in Section 3, and finally the characterization results are presented in Section 4.

2. DESIGN CONSIDERATIONS

(1) Working basics

Figure 1 is a cross section view of one layer of the LC beam deflector. A thin layer of nematic LC is sandwiched between a polymethyl-methacrylate (PMMA) blazed grating and a transparent cover plate. The transparent metal indium tin oxide (ITO) layer deposited underneath the PMMA grating and another ITO

Part of the SPIE Conference on Advanced Optical Memories and Interfaces to Computer Storage • San Diego, California • July 1998
SPIE Vol. 3468 • 0277-786X/98/$10.00

layer coated on the bottom surface of cover plate are used to electrically drive the LC to change the phase information of the transmitted light. The essential idea to operate this LC/PMMA composite grating is to exploit the electro-optic effect of nematic LC,[3] where its refractive index for extraordinary light can be continuously changed with the applied voltage. When no electric field is applied, the refractive indices of the PMMA substrate and LC are different, so that strong diffraction can be induced in this "OFF" state. The diffraction efficiency (**D.E.**) is determined by the grating parameters, such as depth, period, and blaze profile. When an electric field is applied, the refractive index of the LC is decreased, resulting in "index matching" between the PMMA and LC. The whole structure can then be considered as an optical flat plate, so that no diffraction occurs in the "ON" state. Hence the beam can either be deflected (the LC "OFF" state) or undeflected (the LC "ON" state).

The final beam deflector consists of a stack of LC blazed gratings with different grating periods. When stacking, the top grating's period is made to be twice the period of the bottom grating to make all steering angles clearly resolvable. By applying different driving conditions on each layer, multiple steering angles are easily achieved. Figure 2 illustrates the concept to realize multiple steering angles. The output can be one of four different outputs depending on different driving condition combinations. Obviously, the multiple angle deflector's **D.E.** is strongly depended on the each layer's **D.E.**. In addition, this LC device is a polarized beam deflector because the above-described electro-optic mechanism only works for extraordinary polarized light.

(2) Blazed grating diffraction analysis

To understand the behavior of this device, an analysis of the blazed grating diffraction is required. Considering the relatively large feature size of the device, a scalar theory analysis[4] can be used. In this analysis, the aperture transmittance of the blazed grating is considered as a prism function P(x) (see Figure 3) convolved with a periodic grating function G(x):

$$T(x) = P(x) * G(x) \tag{1}$$

where

$$G(x)=\sum_{m}\delta(x-mp)\,\mathrm{rect}(x/A) \tag{2}$$

For the prism function P(x), the defect at duty cycle is also taken into account. So

$$P(x)=\mathrm{rect}(x/p)\exp(i\Delta(x)) \tag{3}$$

where $\Delta(x)$ is defined as

$$\Delta_1(x) = 2\pi(n_1-n_2)x\tan\theta/\lambda \quad (0<x<a) \tag{4a}$$
$$\Delta_2(x) = 2\pi(n_1-n_2)d/\lambda \quad (a<x<p) \tag{4b}$$

Then the far field is the Fourier transform of this aperture transmittance,

$$E(x) = \text{F.T. } \{T(x)\} = \text{F.T.}\{P(x)\} \bullet \text{F.T. } \{G(x)\} = \mathbf{P} \bullet \mathbf{G} \tag{5}$$

Obviously, **P** results in a sinc function profile in the far field and its peak location is defined by the prism depth d. **G** defines the diffraction order locations and samples the prism-produced sinc function to define the final diffraction pattern. If the blazed grating is well designed so that the prism-produced Sinc function profile peaks at 1st diffraction order position, then theoretically the 1st order will have 100% **D.E.** and all other diffraction orders will have zero **D.E.**. For our LC/PMMA blazed grating, the optimal design depth is calculated to be 2.67um with a ideal profile (100% duty cycle).

(3) LC electro-optic effect

A detailed analysis of the LC is also required since it plays a key role for dynamic steering. Normally the LC needs to be aligned to work properly. The homogeneous aligned nematic configuration (Figure 4) is chosen for our deflector. When the driving voltage is applied, the LC molecule director tends to align itself along the electric field direction. According to Frank elastic continuum theory,[3] the LC molecule director distribution will be stable when its net free energy is minimized. The net free energy $\mathbf{F}_{net}$ of LC molecule director is represented as

$$\mathbf{F}_{net} = \int_0^L \{ \mathbf{K}_{11} (\nabla \bullet \mathbf{n})^2 + \mathbf{K}_{33} [\nabla \times (\nabla \times \mathbf{n})]^2 - \mathbf{D} \bullet \mathbf{E} \} \, dz \qquad (6)$$

Where $\mathbf{n}=(\cos\theta, 0, \sin\theta)$ is the LC molecule director, θ is the director orientation angle, $\mathbf{K}_{11}$ and $\mathbf{K}_{33}$ are the LC splay and bend elastic constant respectively, $\mathbf{D}$ is the electric displacement and $\mathbf{E}$ is the electric field. A numerical simulation was performed to predict the director distribution at different driving voltages. From this distribution, the refractive index information of LC can be easily obtained. Figure 5 shows the simulation results. The refractive index decreases with driving voltage after passing through the threshold voltage, which is about 1V for E7 LC.

(4) Driving voltage loss and non-uniformity

For our device, the driving voltage is applied between two ITO layers. However, the PMMA grating is made on top of the ITO layer of the bottom glass to simplify the fabrication process. This obviously will reduce the voltage on the LC since PMMA is not a good conducting material. Also the PMMA grating profile results in different applied voltages on the LC at different locations. (Figure 6)

The following voltage loss calculation can be used to determine the voltage applied across the LC. Maxwell's equation boundary condition for electrical fields is

$$\mathbf{D}_{LCn} - \mathbf{D}_{PMMAn} = \sigma = 0 \qquad (7)$$

Where D is the displacement and σ is the net free charge density which is zero in our analysis. The dielectric constants of LC and PMMA are about 18 and 3 respectively. Considering that there is a residual PMMA layer at the bottom of LC/PMMA grating, the effective voltage $\mathbf{V}_{eff}$ on LC/PMMA grating can be obtained by the following equation:

$$\mathbf{V}_{eff} = (1 - \mathbf{r}) / (1 + 5\mathbf{r}) \, \mathbf{V}_{apply} \qquad (8)$$

Where $\mathbf{V}_{apply}$ is the applied voltage and $\mathbf{r}$ is the ratio of the residual PMMA layer depth and the depth summation of spacer and PMMA grating. From this we can define the real voltage on the LC $\mathbf{V}_{LC}$ at different positions:

$$\mathbf{V}_{LC} = (1 - \mathbf{rr}) / (1 + 5\mathbf{rr}) \, \mathbf{V}_{eff} \qquad (9)$$

Where $\mathbf{rr}$ is the depth ratio between PMMA grating and spacer at different locations. From calculations, only 18% to 60% of the driving voltage is applied on the LC with the parameters of 5μm spacer, 0.6μm residual uniform PMMA layer, and PMMA grating depth of 2.67μm.

The phase delay caused by the LC/PMMA composite structure at different locations within one period was calculated at different applied voltages. Figure 7 shows that, although the voltage on the LC is different at different positions, the phases at those positions actually become more uniform at higher voltage. The reason is that the refractive index of LC is decreased at higher voltage, so that the phase delay gets compensated. This analysis improves our understanding of device's working principles in the "ON" state. Normally, it is difficult to reach index matching between LC and PMMA at every location due to the applied voltage's non-uniform distribution. However, we can reach uniform phase distribution at every

location at a higher voltage, which ensures the device's successful operation. In that sense, it is more meaningful to discuss the phase matching rather than the index matching.

3. FABRICATION PROCESS

The PMMA blazed gratings were fabricated by direct-write electron-beam lithography.[5] The ITO-coated substrates were prepared by spinning in succession five layers of PMMA to achieve a total thickness of ~3.3 μm. Each deposition sequence included a bake-out for 60 minutes at 170º C. Prior to exposure, the sample was overcoated with 100 Å of aluminum, which acted as a discharge layer preventing defocusing due to surface charge buildup. The E-beam exposure patterns for the blazed gratings were composed of square pixels (0.5 μm for 5 μm period grating, 1 μm for 10 μm period grating). Within each pixel, the E-beam spot was rastered to uniformly expose the pixel area. The pixel doses were determined from the desired depths, taking into account the nonlinear depth versus dose response of the PMMA and the E-beam proximity effect (backscattered dose from the substrate). The proximity effect for these substrates (50 kV acceleration voltage) was measured[5] to have a Gaussian 1/e radius of 10.75 μm and an integrated strength of 0.5 of the initial dose. Fourier transform deconvolution of the proximity effect function was performed on the pixelized dose profile as described in Ref. 5.

The gratings were exposed using a JEOL JBX-5DII E-beam lithography system at 50 kV with a beam current of 4 nA, which corresponds to a spot size of ~0.3 μm. This is larger than would be used for precision lithography, but it somewhat smoothes the surface of the blazed grating and reduces writing time. The total exposure time for each grating having an area 3.2 mm x 3.2 mm area was 70 minutes. After exposure, the aluminum overcoat was removed and the grating was developed in pure acetone using a Solitec spinner equipped with an electronically controlled Tridak resist dispenser. The substrate was spun at 1000 RPM while the acetone was squirted down at the center of rotation. At the end of 8 seconds, the acetone was abruptly cut off and replaced by a blast of dry nitrogen. This quenched the development and at the same time dried the surface of the PMMA. Additional development steps with times as short as 0.5 seconds were used to achieve the desired grating depth. The depth was gauged by measuring the diffraction from a computer-generated hologram (on the same substrate) that was designed to produce a null zero order. Near the final depth, the grating profile was measured directly using a Digital Instruments Nanoscope III atomic force microscope. Figure 8 shows the final surface profile of the 10 micron period grating.

The LC filling process for PMMA blazed grating is described below. First, a glass plate is coated with a 20 Ω/≤ indium-tin-oxide transparent electrode to form the ITO glass. A polyimide solution (1% mass in NMP) is spun onto the ITO glass at 3000 rpm for 40 second and then baked at 200°C for 30 minute. The ITO glass is rubbed unidirectionally on a cloth to form a uniaxially buffered alignment layer. This cover glass plate is then affixed to the surface of the PMMA blazed grating, at a microscopic distance set by small drops of a mixture of chopped glass fibers and Norland61 UV-cured optical adhesive deposited on the periphery of the active area of the grating. The resulting cavity is filled with Merck E7 in nematic phase. The filling process has to be finished in room temperature since the PMMA pattern can't withstand high temperature.

In the above process, we did not coat and rub the PMMA grating surface to get the homogeneous alignment as we did for the cover plate. The reason is that the E-beam fabricated blazed grating surface had tiny grooves (see Fig. 8) that can be utilized as the natural alignment layer if we fill LC along these grooves' direction. It is important that the cover plate's alignment direction must be parallel to the grating groves direction to reach the homogeneous alignment configuration.

4. Experiment and Discussion

For the experimental setup, a polarized beam was incident on the deflector with its polarization parallel to the LC alignment direction since it is a polarized beam deflector. Two DC-balanced 1KHz square

waveforms are applied onto two LC blazed gratings respectively. A detector mounted on a scanning translation stage measures the far field intensity at each spot to get the **D.E**.

First, we determined the PMMA blazed grating profile by combining three measurements. The first step is to use the AFM profile measurement data (Fig. 8). However, the tip of AFM does not probe the deepest corner of the grating, so the depth measurement is not reliable. Nevertheless, it did accurately give us duty cycle information, which is used for the next two approaches. The second step is to compare the experimental and theoretical prediction for the diffraction of PMMA blazed grating in free space. We then filled LC into the PMMA blazed grating and proceed the third step, which is to compare the experimental and theoretical prediction for the diffraction of the LC/PMMA composite grating without any applied voltage. The two fabricated PMMA blazed grating profiles' parameters were determined to be as follows: for the 10μm period sample, the depth is ~2.74μm and the duty cycle is ~82%; for the 5um period sample, the depth is ~2.85um and the duty cycle is ~90%.

Next, we measured the intensity variations while scanning the driving voltage from zero to 8V for the two LC blazed gratings. As we can see from Figure 9, the **D.E.** at a small voltages (1.5V and 2V for the 10μm and 5um samples respectively) are even higher than that at zero voltage for the OFF state. The reason is that the device's depth is slightly higher than the design optimal depth. As was discussed above in the scalar theory analysis, the prism produces a Sinc function which could shift the blaze at different diffraction orders with different prism depth,

$$\delta = 2\pi\Delta n \times d / \lambda \qquad (10)$$

where δ is the phase difference, Δn is the refractive index difference between PMMA and LC, λ is the illumination wavelength. If the depth d is slightly larger than the optimal one, δ is larger than expected so that peak will be located to the right side of the desired position. We can shift the Sinc function peak back to the right order through keeping the same δ by reducing Δn. This can be done for LC since its refractive index can be lowered by applying a small voltage. We call this small voltage as "virtual" OFF voltage of the LC deflector.

The above discussion also gives us a hint for the device fabrication. Actually what we should really care about during PMMA blazed grating fabrication is the grating shape rather than the strict control of depth. As long as its depth is larger than the optimal design goal, the defect can always be compensated by using a "virtual" OFF voltage. This property helps us during the fabrication since accurate control of the depth is somewhat painstaking. (Of course, the depth can not exceed the design goal too much since it might cause other problems for the beam steering, say, the PMMA depth is large and the voltage loss is big so that a very large ON voltage will be needed to reach phase matching. Or, the depth is so large that the grating will be blazed at other higher orders, etc.)

Using this "virtual" OFF voltage trick, we first tested the two LC deflectors separately. The maximum applied voltage is 15V, considering that the voltage loss calculated before, the real voltage on LC is about 2.7V to 9V. For each deflector, the measured **D.E.**s at ON and OFF state are all in the range of 81.7% to 88.6%. The crosstalk turns out to be very small. (The intensity ratios between the brightest spot and the second brightest spot are in the range of 32~41) After that, we stacked the two deflectors together to form a four-angle deflector. The measurement data in Figure 10 shows that the steering efficiencies of those four angles are ranged from 66% to 75%. The intensity ratio between the strongest and second strongest spots is in the range of 13~21. The data from the characterization experiments are listed in Table 1. Finally, Figure 10 shows the beam steering spots. Four steering angles (10.8°, 7.2°, 3.6°, 0°) are obtained with a resolution of 3.6 °.

Table 1. Measured Diffraction Efficiencies (%) of the Liquid Crystal Blazed Grating Deflector

Diffraction Order	10μm period		5μm period		Both ON	5μm ON 10μm OFF	5μm OFF 10μm ON	Both OFF
	OFF	ON	OFF	ON				
-3	1.82	0.56	1.81	0.84	0.70	4.21	0.66	**65.02**
-2	0.84	0.57	2.05	1.34	3.51	0.76	**71.21**	0.82
-1	**82.90**	2.64	**81.68**	2.40	2.40	**72.15**	2.63	4.53
0	2.03	**88.62**	2.56	**87.65**	**75.36**	3.31	4.29	1.93
1	0.53	2.47	2.15	2.30	2.36	2.80	2.20	4.76
2	0.85	0.71	2.48	1.40	3.70	1.05	2.64	1.87

5. CONCLUSION

A multiple-angle liquid crystal blazed-grating beam deflector has been developed. Four steering angles with approximately 70% diffraction efficiency have been demonstrated. At the same time, a detailed analysis of LC/PMMA blazed grating deflector has been carried out, which provided excellent guidance during the deflector's development procedure. A new multiple-angle deflector with much more powerful addressing capability is also being developed.

6. ACKNOWLEDGEMENTS

This work was supported by Air Force Rome Lab and NSF/ERC for neuromorphic systems engineering.

7. REFERENCES

1. J. Thomas, M. Lasher, Y. Fainman, P. Soltan, "PLZT-based dynamic diffractive optical element for high-speed random-access beam steering," SPIE Proceedings vol. 3131, p124, 1997.
2. D.Resler, D.Hobbs, R.Sharp, L.Friedman, T.Dorschner, "High efficiency liquid crystal optical phased array beam steering," *Opt. Lett.*, Vol. 21, No.9, p 689, 1996.
3. L.M.Blinov, V.G.Chigrinov, *Electrooptic effects in liquid crystal materials*, Chap 4, Springer-Verlag, New York, 1994.
4. J.W.Goodman, *Introduction to Fourier Optics*, McGraw-Hill, 1968.
5. P. D. Maker, D. W. Wilson, and R. E. Muller, "Fabrication and performance of optical interconnect analog phase holograms made be E-beam lithography," in *Optoelectronic Interconnects and Packaging*, R. T. Chen and P. S. Guilfoyle, eds., SPIE Proceedings vol. CR62, pp. 415-430, Jan. 1996.

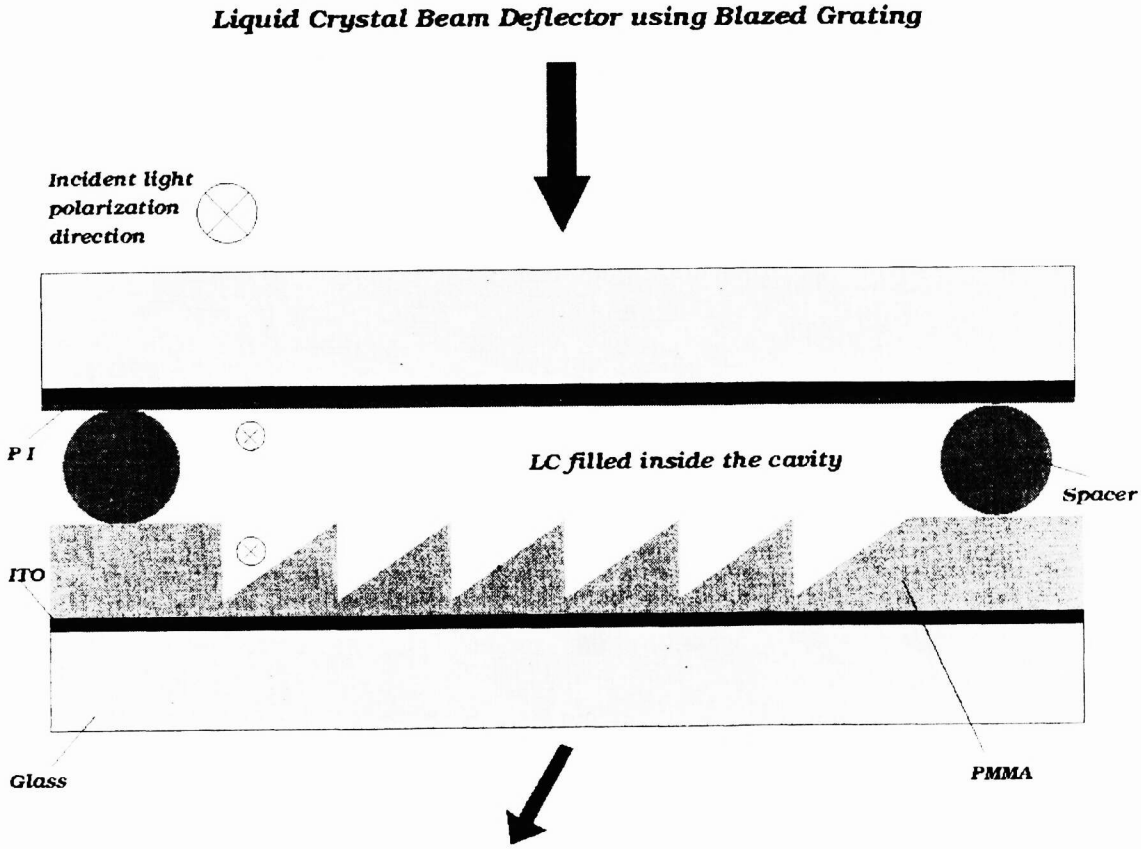

Figure 1. Liquid Crystal blazed grating beam deflector

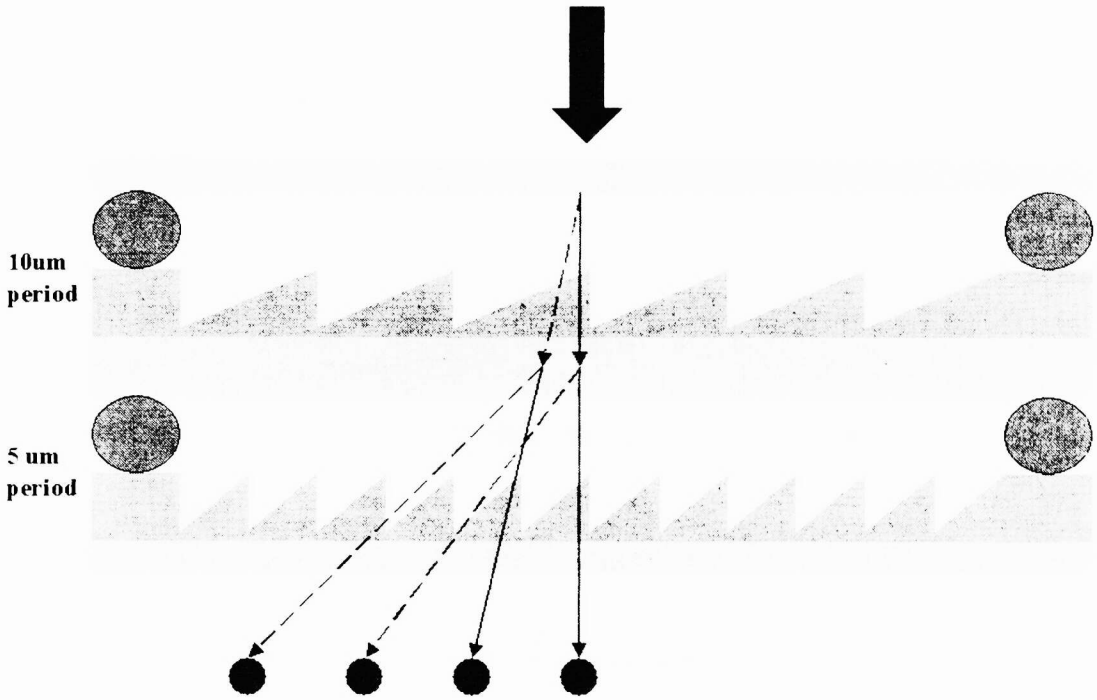

Figure 2. Multiple angle beam steering concept.

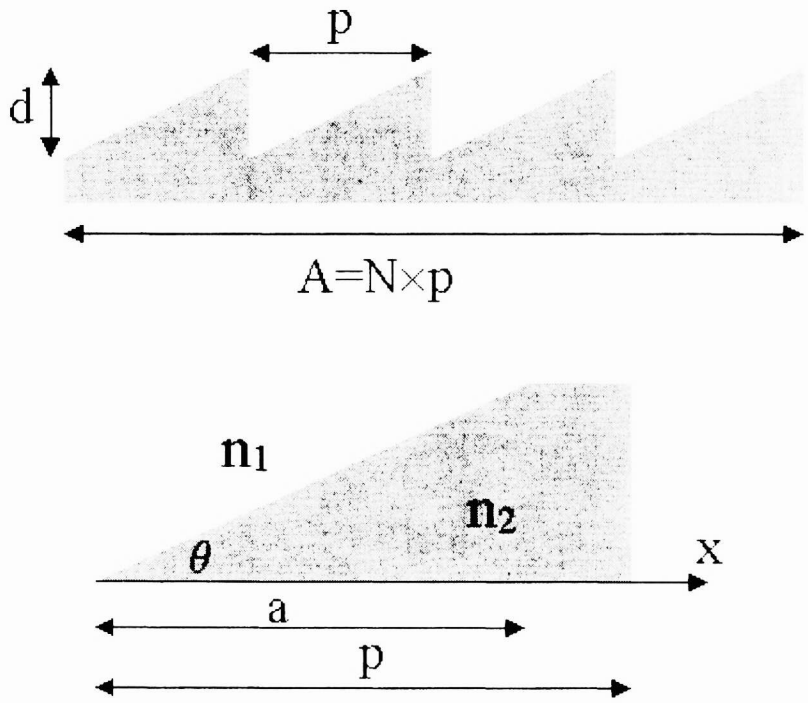

Figure 3. Blazed grating scalar theory analysis.

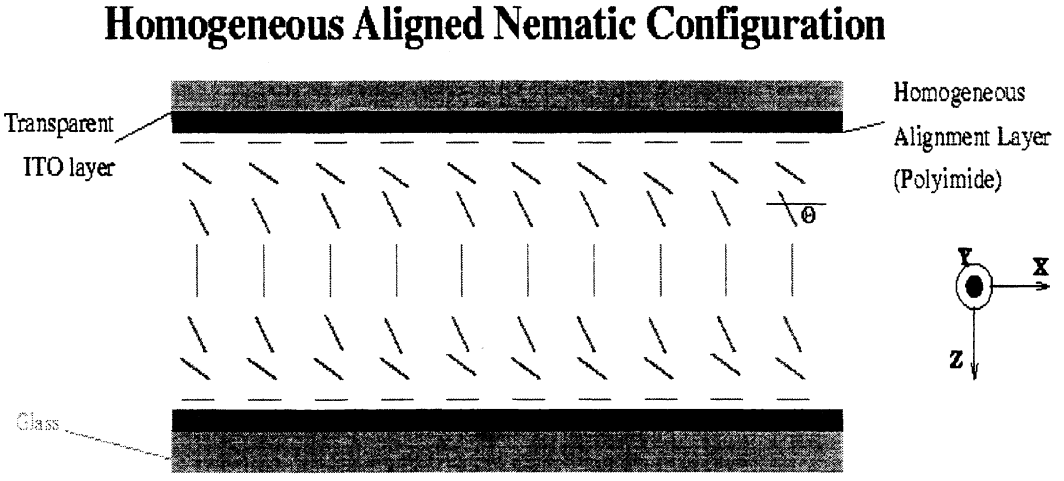

Figure 4. Homogeneous aligned nematic configuration.

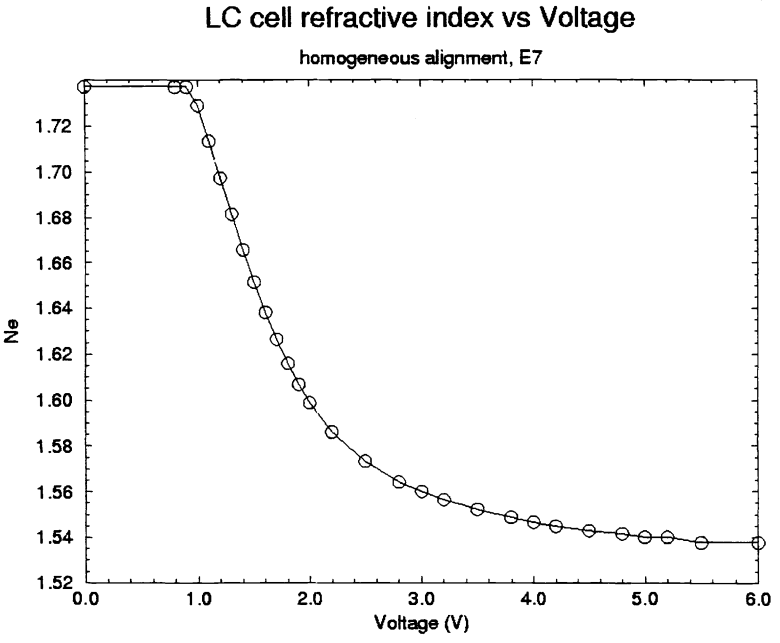

Figure 5. Liquid Crystal cell refractive index vs voltage.

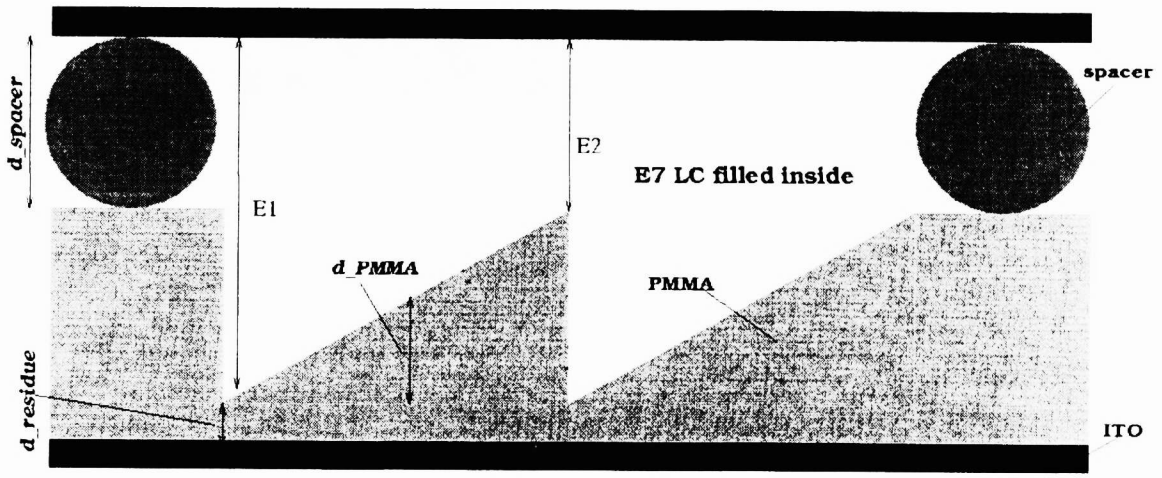

Figure 6. Liquid crystal deflector voltage loss and non-uniformity.

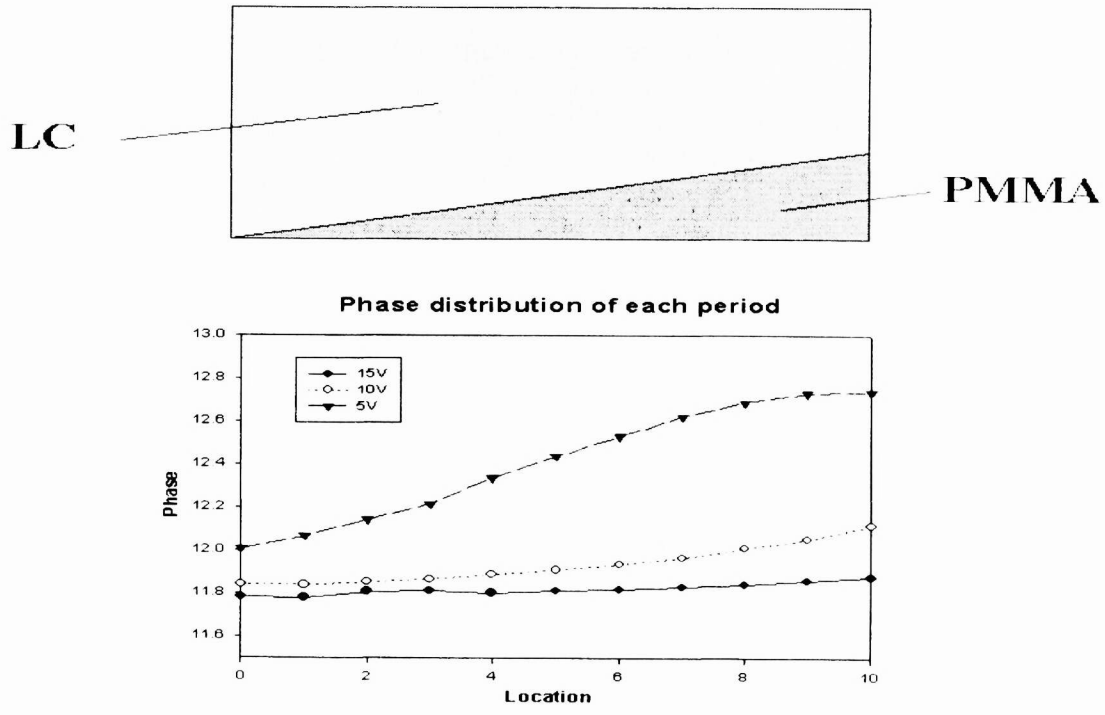

Figure 7. Liquid Crystal deflector phase delay vs location within one period

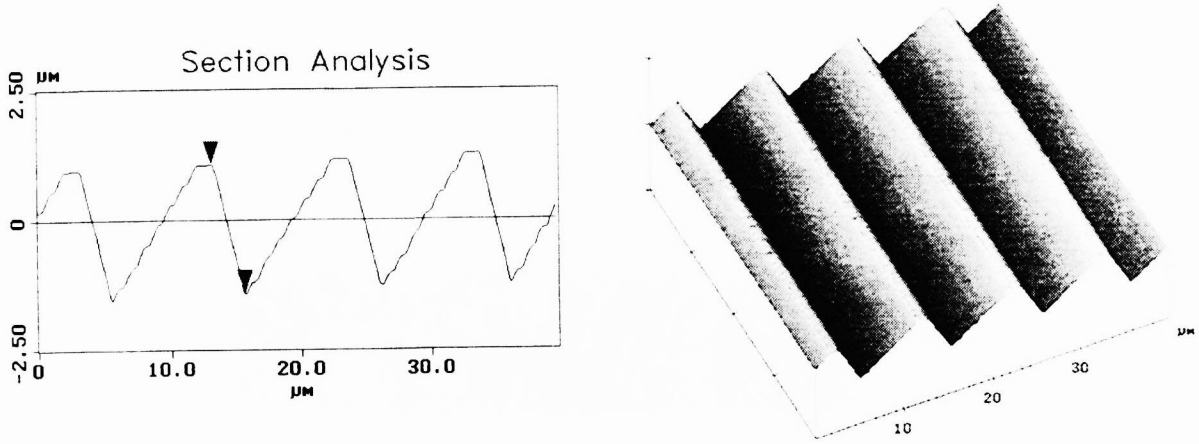

Figure 8. Surface profile of 10um PMMA blazed grating.

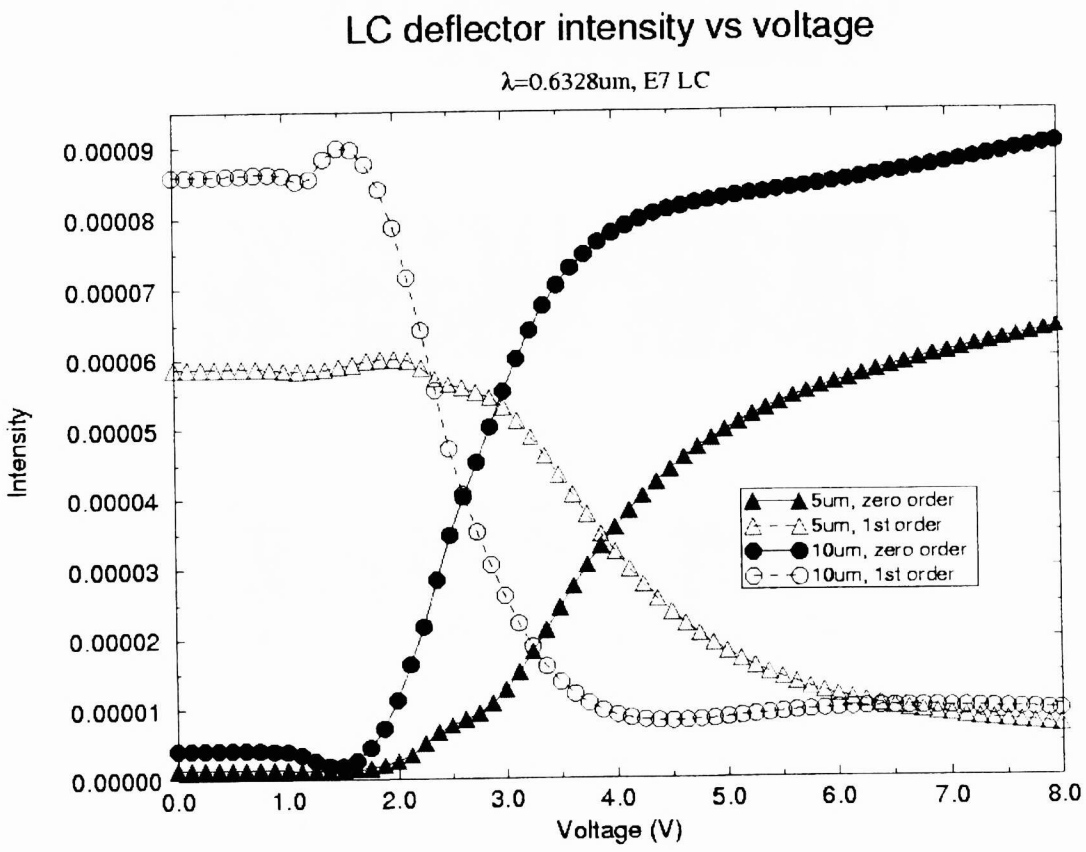

Figure 9. Liquid Crystal deflector intensity vs voltage

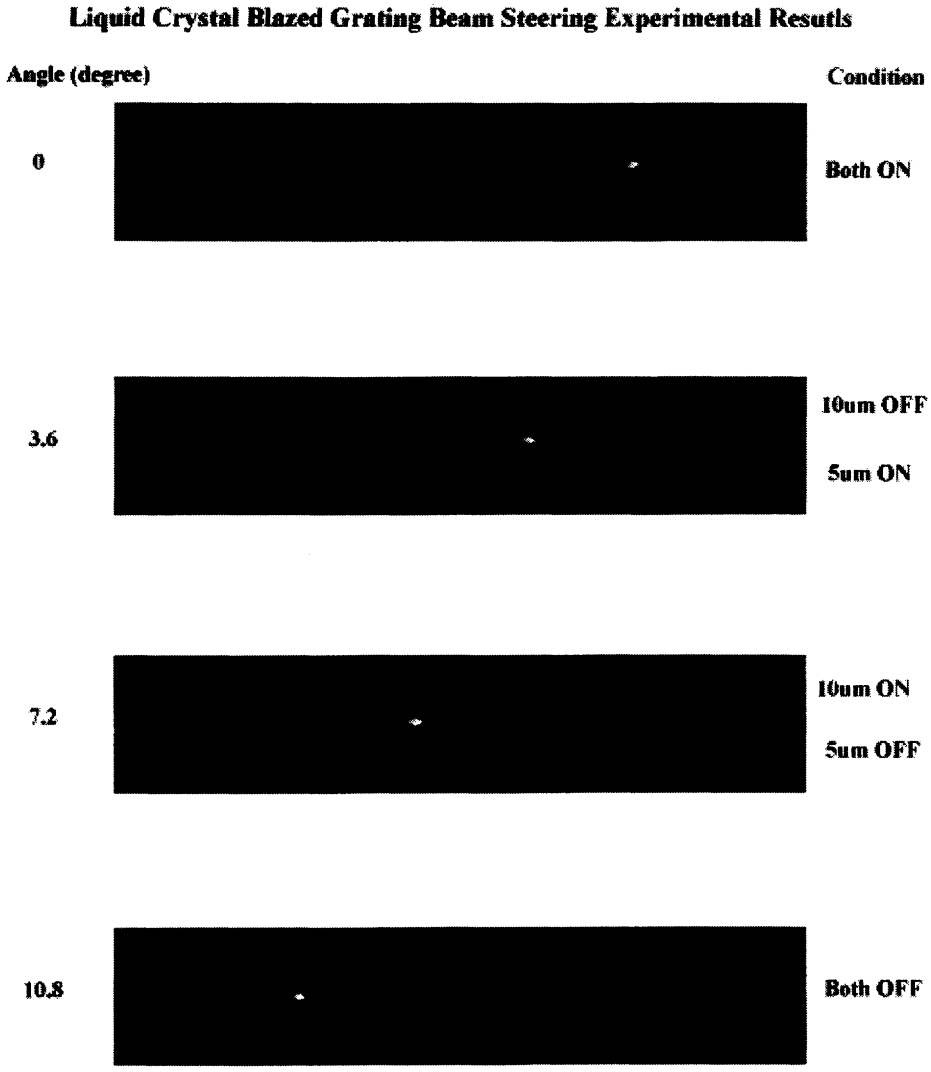

Figure 10. Multiple angle addressing beam spots.